

Konrad-Zuse-Zentrum
für Informationstechnik Berlin

Takustraße 7
D-14195 Berlin-Dahlem
Germany

WERNER BENGER

HANS-CHRISTIAN HEGE

The Tensor Splats Rendering Technique

Tensor Splat Rendering Technique for Tensor Fields

Werner Bengert^{1,2*}

Hans-Christian Hege^{1†}

¹Zuse Institute Berlin, D-14195 Berlin-Dahlem, Germany

²Max-Planck Institute for Gravitational Physics, D-14476 Golm, Germany

Abstract

A new visualization technique for the visualization of symmetric positive definite tensor fields of rank two is introduced. It is based on a splatting technique that is build from tiny transparent glyph primitives which are capable to incorporate the full directional information content of a tensor. The result is an information-rich image that allows to read off the preferred directions in a tensor field. It is useful for analyzing slices or volumes of a three-dimensional tensor field and can be overlaid with standard volume rendering or color mapping. The application of the rendering technique is demonstrated on general relativistic data and the diffusion tensor field of a human brain.

CR Categories: I.3.3 [Computer Graphics]: Picture/Image generation—Viewing algorithms; I.3.7 [Computer Graphics]: Three-Dimensional Graphics and Realism—Color, shading, shadowing, and texture; J.2.9 [Computer Applications]: Physical Sciences And Engineering—Physics

Keywords: tensor field visualization, metric, splatting, volume rendering, general relativity, diffusion tensor images

1 Introduction

Tensor fields are the primary computational quantities in general relativity, they also occur in material sciences as well as in computational fluid dynamics, and with the recent advances in magneto-resonance equipment also in medicine as diffusion tensor images. Unfortunately, appropriate visualization tools are not widely spread, and even people working with tensor fields sometimes think of them as purely abstract objects or as a collection of numbers, which are inspected separately. However, a tensor should always be treated as an entity and visualized without reduction to single scalar or vector fields, because all such reductions impose information loss. Hence the difficulty of visualizing six quantities per point in a data volume, even in the simplest case of a symmetric tensor field of rank two. Nevertheless appropriate visualization methods are required, once for the scientist who needs to inspect data quantitatively or qualitatively for data-mining purposes in huge data sets, but also for public outreach, which is especially important for abstract sciences like general relativity.

In this paper a rendering technique for tensor fields of rank two on three-dimensional manifolds is described. Section 2 starts with a review of the current tensor field visualization strategies. Section 3 explains the idea to replace point-wise glyphs by transparent splats. The resulting images are interpreted in section 4 on the basis of tensor fields from general relativity: in section 4.1 the analytically known Schwarzschild metric describing the gravitational field of a static black hole, in section 4.2 a rotating black hole (Kerr metric), and finally in section 4.3 a numerical solution of two orbiting black holes. To demonstrate that the developed technique is not limited to relativistic data, it is applied to the diffusion tensor field of a human brain in section 5.

2 Related Work

Usually tensor fields visualization work concentrates on symmetric tensor fields of rank two in three dimensions. Only few approaches exist to deal with general three-dimensional tensors rank two or even higher rank [16]. Most visualization methods are constrained even more to the domain of positive definite tensors. The most straightforward way of visualizing these is done by ellipses (in 2D) and ellipsoids (in 3D). Alternative icons have been invented to enhance certain properties more clearly, like the Haber Glyph [11] and the Reynolds Glyph [20].

A problem common to all visualization techniques using icons is visual clutter, an experience which is tackled in vector field visualization by visualizing critical points and integral lines, like streamlines, streaklines and pathlines. Hyperstreamlines [10] are streamlines of the maximum (or minimum) eigenvector “field” with an elliptical cross-section encoding the median and minor eigenvalues. Together with color coding of the maximum eigenvalue they depict all 6 independent components of a symmetric tensor field. It may also be extended to asymmetric tensor fields by drawing a cross instead of an ellipsoid. However, integration of an eigenvector “field” runs into problems

*benger@zib.de

†hege@zib.de

in isotropic regions of a tensor field, where the maximum eigenvector becomes undefined (similar “isotropy artefacts” also happen with the previously mentioned glyph methods that are designated to enhance anisotropy) – an integral line of the maximum eigenvector field may therefore may wildly jump from point to point. Tensorlines [28] intend to cure this problem by weighting the influence of the eigenvector field along an integral line by the isotropy of the tensor field at each integration point.

The quality of integral lines strongly depends on the initial seeds and depicts just a subset of the complete data volume. Volume rendering [14, 15] of tensor fields by mapping tensor field quantities to colors and shading parameters provides more overview of the entire data set, but requires some learning of the visual effects and user interaction within the parameter space.

Deformation fields [5, 6] provide a more intuitive vision by showing the deformation of surfaces under the action of a tensor field. This technique also works for asymmetric tensor fields and can be extended to volumes [32], but is limited to only a fraction of the tensor field at once as it requires some user-chosen input vector field. The full information content of the tensor field is not visualized before it has been probed with three linearly independent vector fields, resulting in three views that have to be mentally combined.

The keystrokes of Van Gogh inspired a technique [17] to draw two-dimensional slices of a tensor field by small normalized ellipses, encoding the trace of the tensor field as a stripe texture on the ellipses. The result is a texture pattern that provides a qualitative overview of the tensor field properties when viewed from a distance, but also provides quantitative details when inspected closely. Drawbacks are its limitation to slices and the built-in property that two eigenvalues are similar. Smearing some spot noise [26] along the dominant directions contained in a tensor field yields images like volume LIC [13], but appears to be computationally expensive and the artificial noise structure adds visual information that is not really contained in the original data.

Another way to look at tensor fields is to interpret them as metric tensor fields, describing physical distances in space (and time). An intuitive interpretation is provided by isometric embeddings [4, 23, 22, 12]. The equivalent of vector field integral lines in a metric field are geodesics [7]. The consideration of lightlike geodesics opens the path to the most physically correct and coordinate independent way of visualizing a metric field by photorealistic images via raytracing in curved space [3, 29], but this approach is computationally very expensive and of limited usability when inspecting simulation data for numerical purposes. A “poor man’s” raytracing approach was recently used [33] by treating integral lines of deviated vector fields as light paths, leading to interesting lensing effects similar to those of relativistic planar refractive objects [18].

3 Rendering Technique

3.1 Mathematical Background

A covariant tensor G of rank two on a manifold M is a bilinear map of two tangential vectors $\vec{v}, \vec{w} \in T_p(M)$ to a number:

$$G : T_p(M) \times T_p(M) \rightarrow \mathbb{R}$$

whereby $T_p(M)$ denotes the tangential space of the manifold M at a point $p \in M$. A straightforward way to look at a tensor in a coordinate-independent way is to consider the set of tangential vectors $\vec{v} \in T_p(M)$ which are mapped to the same number $G(\vec{v}, \vec{v}) = C$ with $C \in \mathbb{R}$. Physically, $G(\vec{v}, \vec{v})$ tells us how fast some propagation of light or fluid occurs in the direction \vec{v} ; the set of neighboring points $p + \vec{v}$ can be intuitively interpreted as a surface of equal propagation, like the set of all points in a distance of one light second, a “unit sphere” as measured with the tensor G .

The coordinate expression in a chart with basis $\{\vec{\partial}_x, \vec{\partial}_y, \vec{\partial}_z\}$ in $T_p(M)$ and a tangential vector $\vec{v} = x\vec{\partial}_x + y\vec{\partial}_y + z\vec{\partial}_z$ is given by

$$G(\vec{v}, \vec{v}) = G_{xx}x^2 + (G_{xy} + G_{yx})xy + G_{yy}y^2 + (G_{yz} + G_{zy})yz + G_{zz}z^2 + (G_{zx} + G_{xz})xz \quad (1)$$

whereby $G_{ij} := G(\vec{\partial}_i, \vec{\partial}_j)$ are the components of the tensor field G in the given chart. They can be written as a matrix (G_{ij}) . Eq. (1) corresponds to the equation of a quadric surface, i.e. an ellipsoid or an hyperboloid, depending on the signs of G_{ij} . It can be computed in any coordinate system by mapping unit vectors $\vec{u} \in T_p(M)$ with $|\vec{u}| = 1$ (e.g. a unit sphere) to

$$\vec{v} = \frac{\vec{u}}{\sqrt{G(\vec{u}, \vec{u})/C}} \quad (2)$$

If the tensor is not positive definite, then \vec{v} becomes complex in certain directions and the quadric surface is hyperbolic. The alternative mapping $\vec{w} = \vec{u} \cdot \sqrt{G(\vec{u}, \vec{u})/C}$ leads to “inverse ellipsoids” and is the basis of Reynolds glyphs [20]. However, the quadric surface does not display the full information content of a general tensor, but only its symmetric part. For now, we will limit ourselves to symmetric tensors because these are the primary data of interest when a metric tensor field in general relativity is inspected, as well as diffusion tensor data are symmetric either. Furthermore, as far as general relativistic spacetimes [24] are considered, we will only inspect the spatial three-dimensional metric of a four-dimensional spacetime here.

3.2 Shape Classification

The properties of the ellipsoid described by eq. (1) can be analyzed by determining the eigenvalues and eigenvectors of the tensor. A symmetric positive definite 3×3 matrix will reveal three real eigenvalues, denoted by $\lambda_{max} \geq \lambda_{med} \geq \lambda_{min} \geq 0$. Its three orthonormal eigenvectors describe the orientation of the ellipsoid, whereby the length of the i -th axis is given by $1/\sqrt{\lambda_i}$, i.e. the largest extent of the ellipsoid is determined by the smallest eigenvalue and vice versa – this is sometimes confused, but is clear from eq. (2). We also notice that by representing a tensor by its eigen decomposition, we also know the quadric surface of the inverse tensor $(G^{ij}) = (G_{ij})^{-1}$ by inverting the eigenvalues $\lambda_i \rightarrow 1/\lambda_i$.

An intuitively useful classification of tensor ellipsoid shapes was given by Westin [31]. We may distinguish among the following dominant cases depending on the relationships of the inverse tensor’s eigenvalues (we employ the inverse tensor’s eigenvalues here for consistency with Westin’s definitions):

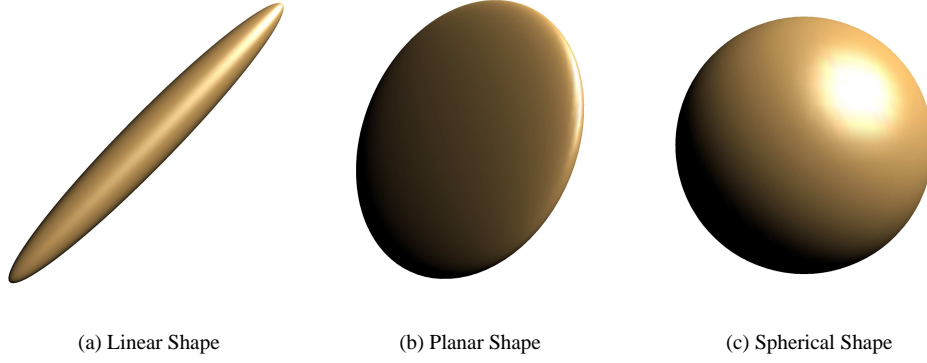


Figure 1: Classification of a tensor ellipsoid by its shape.

- **Linear case:** $\lambda_{max} \gg \lambda_{med} \approx \lambda_{min}$, one eigenvalue of the inverse tensor is dominant. The tensor's ellipsoid is a needle (Fig. 1(a)), the inverse tensor reveals a disc (Fig. 1(b)).
- **Planar case:** $\lambda_{max} \approx \lambda_{med} \gg \lambda_{min}$, two eigenvalues of the inverse tensor are dominant. The tensor's ellipsoid is a disc (Fig. 1(b)), the inverse tensor a needle (Fig. 1(a)).
- **Spherical case:** $\lambda_{max} \approx \lambda_{med} \approx \lambda_{min}$, all eigenvalues are of approximately the same size. No direction is preferred (isotropic case), the tensor and inverse tensor ellipsoids are both spheres.

Westin [31] introduced shape factor definitions as indicators which of the three cases is dominant. They only depend on the ellipsoid shape, independent from its size:

$$\begin{aligned}
 c_l &= \frac{\lambda_{max} - \lambda_{med}}{\lambda_{max} + \lambda_{med} + \lambda_{min}} \\
 c_p &= \frac{2(\lambda_{med} - \lambda_{min})}{\lambda_{max} + \lambda_{med} + \lambda_{min}} \\
 c_s &= \frac{3\lambda_{min}}{\lambda_{max} + \lambda_{med} + \lambda_{min}} .
 \end{aligned}$$

The scaling numbers 2 and 3 are used such that each shape factor is in the interval $[0, 1]$. Other normalization choices are possible as well. The three shape factors obey the relationship

$$c_l + c_p + c_s = 1$$

and can thus be interpreted as barycentric coordinates within a triangle, as illustrated in Fig. 2. The spherical factor c_s is a direct measurement of the anisotropy. The shape factors of the inverse tensor are computed easily by exchanging $c_l \leftrightarrow c_p$ while keeping c_s . Other shape and

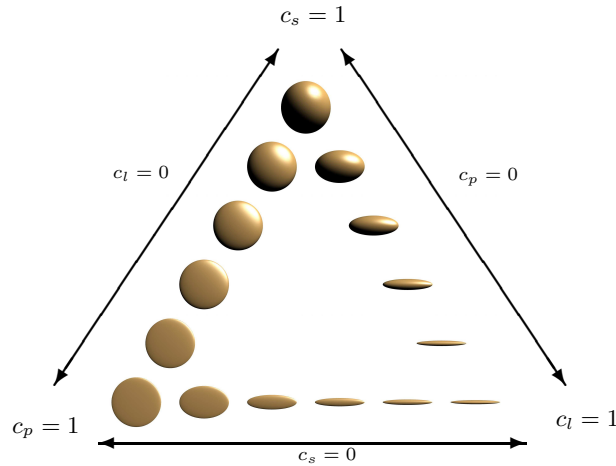


Figure 2: Barycentric shape parameters and their corresponding tensor ellipsoids. The left edge corresponds to zero linearity, bottom edge to zero sphericity and right edge to zero planarity.

anisotropy classifications are possible as well [1], which may even avoid solving the cubic eigenvalue equation [34]. In our case we are interested in the eigenvectors as well, so solving the eigenvalue equation is required anyway.

3.3 Splatting Technique

The idea is inspired from the question: what actually happens in curved space, what is the meaning of the metric tensor field as given in a coordinate volume? The answer is that it specifies the physical distance among neighboring points: even if they might reside regularly distributed in a coordinate space, the distance from one point to another one might be stretched very large, while others are compressed. So the physical grid of points is actually geometrically strongly distorted as compared with the coordinate grid. Unfortunately, a direct geometrical visualization of this behavior by shifting the grid points to directly reflect the physical grid stretching in coordinate space, i.e. computing an isometric embedding of the data volume in flat space, is not possible globally. Even two-dimensional surfaces, e.g. two-dimensional slices through the data volume, cannot necessarily be embedded into flat three-dimensional space globally [4, 23, 22, 12].

An intuitive interpretation of the grid stretching is like a “density” of physically equidistant points in a coordinate cell. A nice way to visualize density fluctuations as they occur in nature is done by the Schlieren photography [25], see Fig. 3 for an example, which is capable to display small density fluctuations in the air as brighter and darker regions. However in contrast to a true (scalar) density, this one “depends

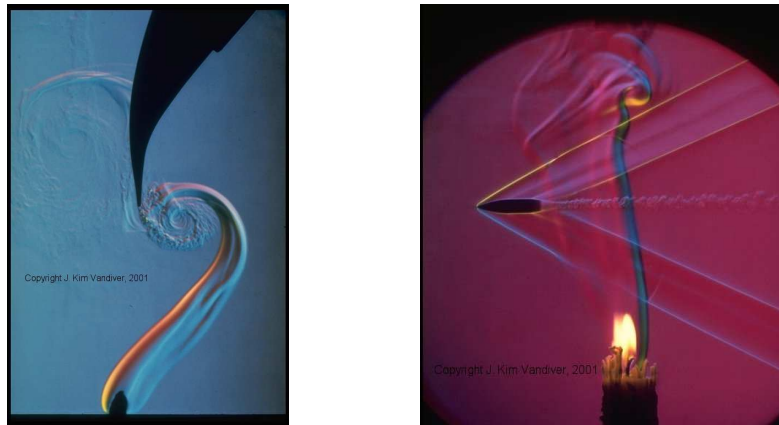


Figure 3: Schlieren photography: Small fluctuations in the density are enhanced by a special point-like intense light source. Images courtesy by J. Kim Vandiver, <http://web.mit.edu/edgerton/people/vandiver/schlieren.html>.

on the direction”. A possible way to visualize this behavior is view-dependent volume rendering (the apparent geometry or volume rendered data set changes with the view point or the rotation of the object), but practical experience showed that this technique tends to be too confusing to the human viewer. Now Schlieren photography is also able to display the small convections of flowing air as sharp, small crisp details, thus encoding also directional information, i.e. the flow direction of the air in addition to the density fluctuations. So ideally a rendering technique for tensor fields could copy this impression: display density fluctuations and encode directional information at the same time.

In [30] a combination of a line segment, a disc and a sphere were used to draw an icon at each vertex point. Each of these icon components is scaled by the respective shape factor, yielding mostly spheres in regions of high isotropy, discs in regions with dominant planarity and line segments in mainly linear regions. Combinations of these icons show the relative size of these components. It gives correct visual impressions for isotropic regions, because the (undefined) maximum eigenvector does not contribute to the spherical icon component. However, opaque icons suffer from view occlusion problems when applied to complex three-dimensional data volumes.

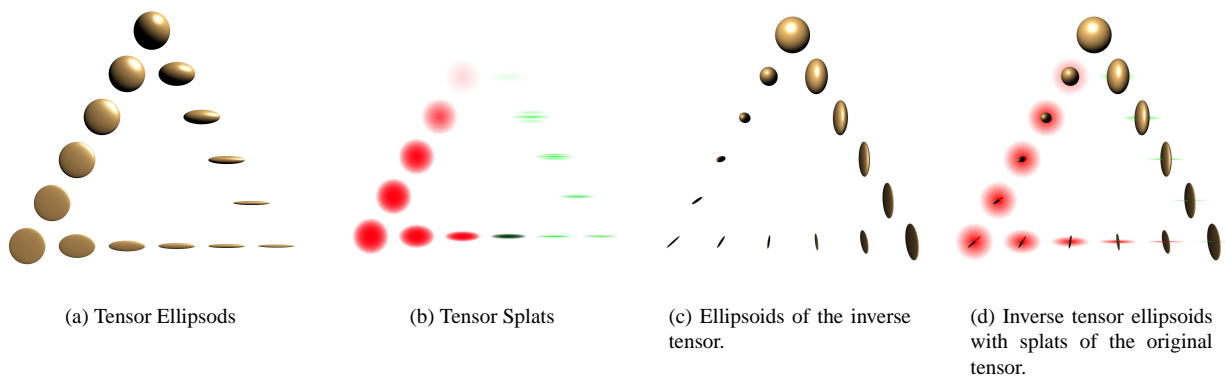


Figure 4: Legend of the glyphs of the tensor and its inverse. Ellipsoids incorporating the tensor field’s value at each point in space is replaced by transparent textured splats. Isotropic regions are rendered transparently to discard any visual directional preference there. The glyphs of the inverse tensor are always orthogonal to the original tensor, whereby linear and planar shape factors are exchanged.

Thus our idea is to replace opaque icons by transparent ones, i.e. splats which fade out and may also overlap, similar as in the spot noise technique[9]. Keeping in mind that we are primarily interested in directional information, it is reasonable to render isotropic regions

completely transparent. As the eigenvectors have no meaning there, the only information available in isotropic regions is the trace of the tensor field, a single scalar, which can also be rendered by standard volume rendering, if of interest at all. Otherwise, in planar regions with two possible directions, a transparent disc with gaussian-like spherical transparency is an appropriate icon, while in linear regions a line segment is appropriate. To blend these two cases we may impose a one-dimensional periodic texture, e.g. some sinusoidal intensity, on the disc which indicates the direction of the larger eigenvector/eigenvalue pair on the dominant plane of the two largest eigenvector/eigenvalue pairs. The texture is scaled by the linearity factor c_l , thus stretched infinitely in planar regions with $q = 0$ and occurring exactly once per splat for $c_l = 1$. The resulting icons are shown in figure 4. They provide the same information as the tensor ellipsoids in Fig. 2.

The one-dimensional texturing on each splat can be freely scaled by a user-adjustable parameter to reveal the most pleasant overall appearance. In regions with non-zero linearity there is thus the freedom to specify how many stripes per splat, or visually “needles per voxel” shall be used for a fixed q value. In any case, regions with higher linearity will be built from more and smaller needles, whereas regions with lower linearity will fade out to smoother appearance. Consequently, since the structural information is rendered with a higher resolution than the original data source, the resulting image should be inspected with higher pixel resolution as the data source.

By interchanging $c_l \longleftrightarrow c_p$ it is easy to switch among a visualization of the tensor field and the inverse tensor field. Both might help to understand the properties of the tensor field, although the physical interpretation might be different. For instance, the tensor field shows the shape of “metric unit spheres” and displays “grid compression”, whereas the inverse tensor stands for “grid stretching” or “flow speed”. Switching from a tensor to its inverse visualization maps linear to planar regions and vice versa, leaving freedom for more pleasing visual appearance to the user.

To enhance the transition from linear to planar regions, we use a colormap depending on

$$c_f := \frac{c_l}{c_l + c_p} \equiv \frac{\lambda_{max} - \lambda_{med}}{\lambda_{max} + \lambda_{med} - 2\lambda_{min}}$$

that specifies the location of a tensor shape on the bottom edge of Fig. 2. The colorization factor c_f becomes undefined in completely isotropic regions where all eigenvalues are identical. However, this does not harm, because isotropic regions are rendered completely transparent (i.e. without issuing any OpenGL directives, thereby also improving rendering speed), such that an eventual color value is irrelevant. Our primary encoding is to use complementary colors, e.g. mapping $c_p = 1$ to red and $c_l = 1$ to green. The actual mapping interval can also be scaled



Figure 5: Color Encoding of c_f , i.e. the $c_s = 0$ line in Fig. 2.

to a subinterval such that even slight variations of the anisotropy can be enhanced strongly. Other color codings are possible as well, and especially encoding the trace of the tensor field as luminosity together with color hue as linearity measurement is an option.

3.4 Benefits of the Rendering Technique

The tensor splat technique offers the following advantages:

- **No isotropy artefacts:** in contrast to many anisotropy enhancing visualization methods, nothing “weird” happens in isotropic regions, where the eigenvectors become undefined, i.e. no direction is suggested where none is preferred.
- **Grid independence:** The rendering technique works point-wise; it is thus independent from the topological structure of the underlying data discretation scheme and is not limited to uniform cartesian grids, but can be applied directly to tetrahedral grids or adaptive mesh refinement (AMR) data.
- **Applicable to dynamic data:** The technique is completely deterministic, i.e. it does not make use of random noise like in LIC [27, 13], and thus is perfectly suited for time-dependent data, revealing smooth animations.
- **Fast:** The graphics primitives can be put into OpenGL display lists, thus achieving interactive rendering speeds and high-speed interactive animations of large data sets. Furthermore, some rendering parameters – e.g. the number of stripes per splat – can be set outside the display list, thus fine-tuning of the visualization can be done interactively in realtime.
- **Adjustable:** By changing the diameter of the tensor splats, the number of texture stripes per tensor splat and transparency parameters the image can be adjusted from a globally smooth appearance providing a raw qualitative overview of large structures into fine, point-wise icons that can be inspected point by point for data debugging and quantitative analysis of tensor values.

4 General Relativistic Data

4.1 Schwarzschild Metric

As a first test case we inspect the Schwarzschild metric. It describes a static black hole with mass m . In matrix notation, it reads in four-dimensional polar coordinates:

$$\begin{pmatrix} 1 - 2m/r & & & \\ & -\frac{1}{1-2m/r} & & \\ & & -r^2 & \\ & & & -r^2 \sin^2 \vartheta \end{pmatrix} \quad (3)$$

whereby for our visualization purposes we are only interested in the spatial part. We see immediately that the radial eigenvector $\vec{\partial}_r$ is

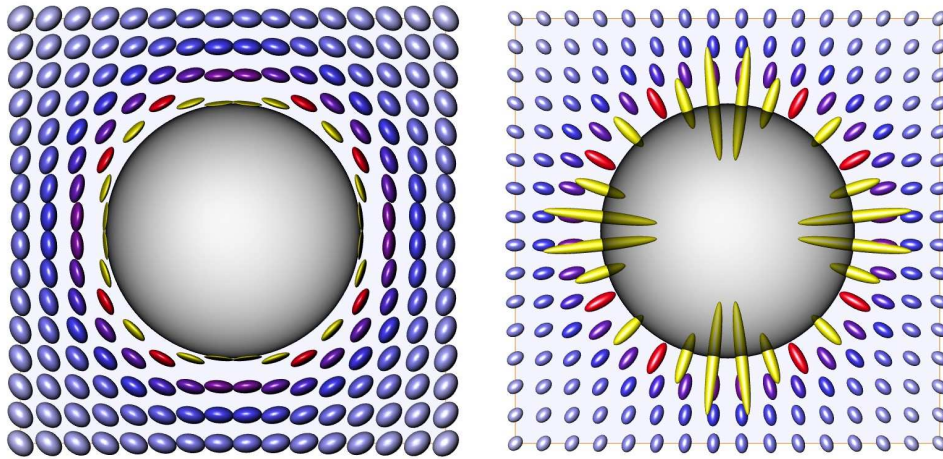


Figure 6: A two-dimensional slice of the spherically symmetric Schwarzschild metric. Tensor ellipsoids (left) visualize light propagation, inverse tensor ellipsoids (right) visualize grid stretching. Colors indicate the trace of the tensor field, the sphere indicates the event horizon.

dominant with eigenvalue $g_{rr} = 1/(1 - 2m/r)$, whereas the angular eigenvalues are exactly like on a sphere, so no direction on concentric spherical shells is preferred. The anisotropy is highest for $r \rightarrow 2m$, the “event horizon” of the black hole. The resulting mostly planar light

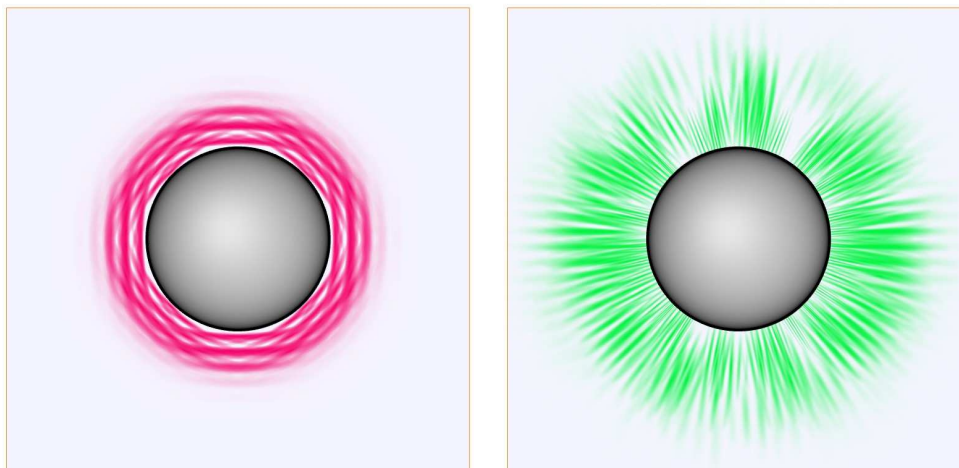


Figure 7: Tensor splats (left: metric tensor, right: inverse tensor) of a 2D slice revealing the radial grid stretching close to the event horizon. Note that the visible discretization artefacts are due to data sampling on a low-resolution uniform cartesian grid.

propagation is easily depicted by the tensor splats as radially oriented planar discs, Fig. 7 (left), whereas the radial grid stretching is displayed by the inverse metric in Fig. 7 (right) as radial needles, indicating the high linearity close to the event horizon.

4.2 Kerr Metric

The Kerr metric, found by accident in the year 1967, describes a rotating black hole with mass m and angular momentum a . In matrix notation, the 4-metric reads:

$$\begin{pmatrix} 1 - \frac{2mr}{\rho^2} & & & \frac{mra \sin^2 \vartheta}{\rho^2} \\ & -\frac{\rho^2}{\Delta} & & \\ & & -\rho^2 & \\ \frac{mra \sin^2 \vartheta}{\rho^2} & & & -\frac{(r^2+a^2)-\Delta a^2 \sin^2 \vartheta}{\rho^2} \sin^2 \vartheta \end{pmatrix} \quad (4)$$

whereby $\Delta := r^2 - 2mr + a^2$ and $\rho^2 := r^2 + a^2 \cos^2 \vartheta$. The condition $a < m$ must hold for a physically reasonable black hole. The case $a = m$ is known as a maximally spinning black hole. For $a = 0$ the Kerr metric is identical to the Schwarzschild metric. For $a > 0$ the Kerr metric is no longer spherically symmetric, but just axially symmetric around the rotation axis. We can see this property reflected in

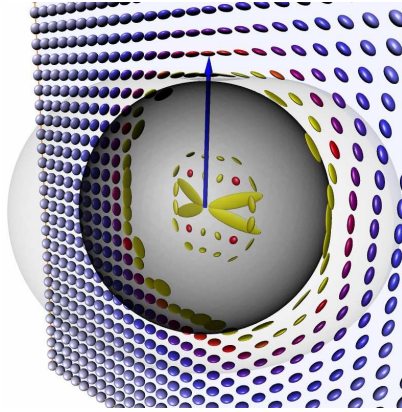


Figure 8: Kerr Ellipses. It is hard to see anything, but with good will we can spot that the ellipses flatten radially and are squeezed longitudinally while stretched axially at the equator.

Fig. 8 and expect linear regions for $a > 0$. Tensor Splats are able to exhibit the contrast among linear (in the equatorial plane) and planar regions (at the poles) quite prominently. We find spherically oriented discs close to the poles; in the equatorial plane they morph to needles parallel to the rotation axis, fig.9. We easily read off that light traversal towards the pole is easier and thus latitudinal distances are shorter than

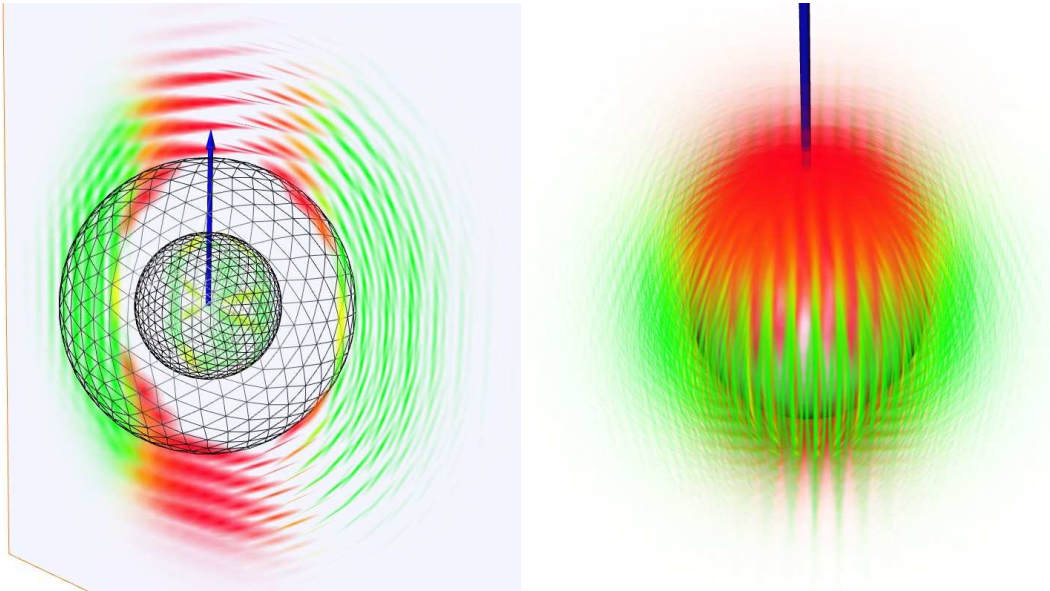


Figure 9: Tensor splats of the anisotropic Kerr Metric. An axial slice (left) and the 3D View (right) expose linear and planar regions, both exhibiting axial linear stretching in the equatorial plane.

longitudinal ones. In other words, the axial stretching close to the equatorial plane indicates that a coordinate sphere is actually a flattened “bubloid”[22, 4] with large equatorial and short polar circumference.

4.3 Numerical Data

For numerical purposes, the four-dimensional field equations are often split into spatial and temporal components. The four-dimensional metric g (10 independent components) is formulated by a scalar α , called the lapse function, a three-dimensional vector field β (3 components), called the shift vector field, and a spatial metric γ (6 components). In matrix notation with indices $i, j \in \{1, 2, 3\}$ the four-dimensional spacetime metric is of the form

$$\begin{pmatrix} \alpha^2 - \sum_{i,j=1}^3 \beta^i \gamma_{ij} \beta^j & -\beta_i \\ -\beta_i & -\gamma_{ij} \end{pmatrix}. \quad (5)$$

In numerical relativity[2], α , β and γ are the primary computational quantities. The spatial metric γ needs to be provided for some initial time and is then evolved with Einstein's equations of the gravitational field. Tensor splats feature a direct visualization of the spatial metric γ . A current research topic is the numerical computation of the final orbit of two black holes before they collide. Of special interest in numerical

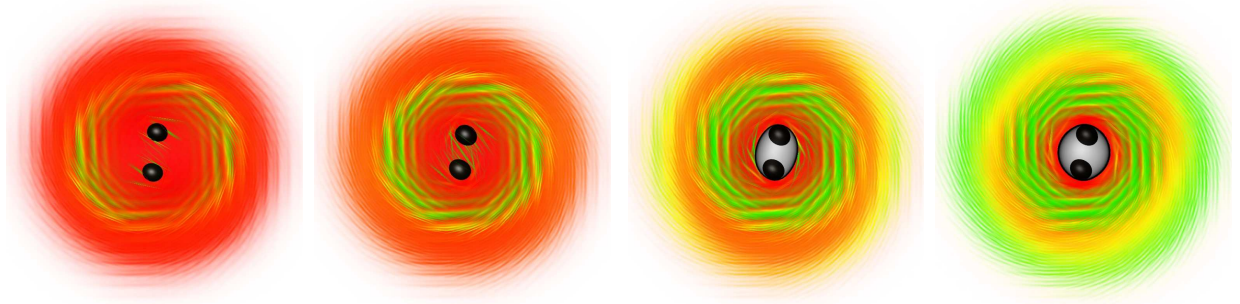


Figure 10: Tensor splats are well suitable for time-dependent data. Two snapshots of a numerical black hole merger sequence, revealing a region of highly linear grid stretching within a region of rather planar grid stretching. Grid resolution is $33 \times 33 \times 17$ points.

relativity is the occurrence of “grid stretching”, the physical distance between neighboring points on the numerical grid, which is determined by the numerically computed metric γ . Due to physical or coordinate singularities they lead to numerical instabilities, ultimately killing the entire simulation sequence. Their early detection and propagation properties are thus essential for the development of improved evolution schemes.

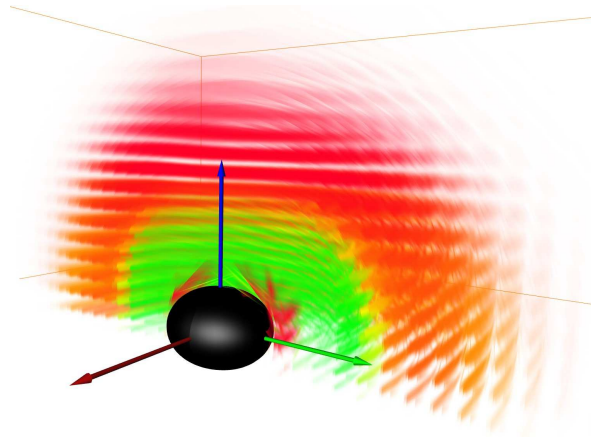


Figure 11: Quadrant with axial slice. At the rotation axis, the grid is stretched only radially, whereas in the equatorial plane grid stretching also occurs in the axial direction.

A quadrant of a dataset just after the merger of two black holes may be analysed using the tensor splats technique. Inspecting the region that is rendered in red in Fig. 11, we find the planar splats oriented radially, thus indicating mainly radial grid stretching, similar to what we know from the Schwarzschild metric. Additionally we see linear grid stretching in the equatorial plane, indicating that light can hardly propagate in the axial ∂_{ϑ} direction. This linearity, a “longitudinal drag”, is stronger close to the black hole, visible as the change of color to green and splat stripes becoming straiter. However, no such green region occurs close to the rotation axis, indicating that there is only radial planar grid stretching. At the pole itself, all tangential directions are equally stretched (no linearity), a symmetry around the rotation axis which we know from the Kerr metric and that is nice to find in the numerical data as well.

The outcome of this is that equatorial circumferences are shorter than polar circumferences, i.e. the true shape of a coordinate sphere is like a cigar along the axis of rotation. Note that computing the actual shape would require determining the embedding [4, 12], but such an embedding does not necessarily exist and could provide insight only for a surface, whereas the tensor splat technique allows to read off geometrical properties of an entire volume (provided its structure is not too complex). The smoothness of visualizing time-dependent data is demonstrated in the second part of the accompanied movie.

5 Brain Data

Diffusion weighted magnetic resonance imaging (DW MRI) is a technique that measures the diffusion properties of water molecules in tissues[34]. Anisotropic diffusion is described by the equation

$$\frac{\partial C}{\partial t} = \vec{\nabla} \cdot (D \vec{\nabla} C) \quad \text{or} \quad C_{,t} = (D^{ij} C_{,i})_{,j}$$

whereby the scalar function $C : M \times \mathbb{R} \rightarrow \mathbb{R}$ is the time-dependent concentration of water molecules and $D : T^*(M) \rightarrow T(M)$ is a symmetric contravariant tensor field of rank two. The inspection of diffusion tensor data is relevant for the segmentation and classification of MRI data to detect the white matter tracts that form the “wiring” of the human brain [15]. Inspection of the measured matrix elements by themselves is not reasonable, because they are not invariant under rotations, hence depending on the scan measurement’s orientation. Invariant visualization methods are thus important here.

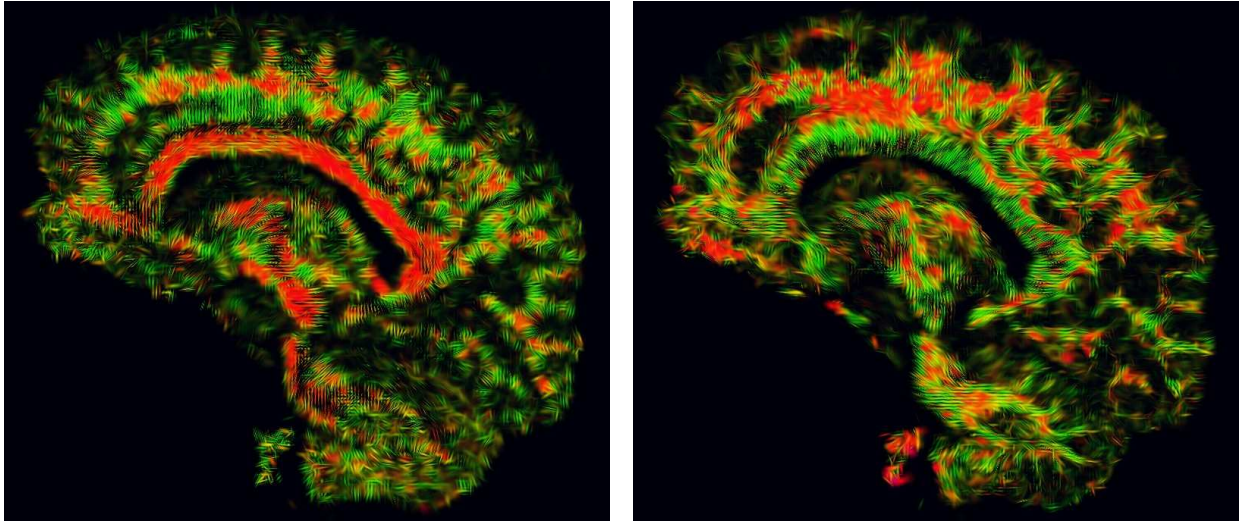


Figure 12: A slice through the brain, displaying diffusion “obstacles”, and the inverse tensor, displaying the possible diffusion velocities. Linear regions are easily detectable, planar regions appear smoother.

Fig. 12 demonstrates the tensor splats technique applied to a two-dimensional slice of a diffusion tensor scan of the human brain with a resolution of $148 \times 190 \times 160$ points. While the coloring provides a rough overview to distinguish among regions with highly linear (water diffusion happens mainly in one direction) and highly planar diffusion (water diffusion may occur in two directions), the finer detailed texture also shows the *direction* of the dominant diffusion. Interactive rotation of a 3D image on a compute screen or stereo viewing in a virtual reality environment provide a better perception of the actual orientation of planar structures. Alternatively, we can also inspect the inverse tensor field, right image in Fig. 12, to map planar splats to linear ones and vice versa. The comparison of both views clearly displays the orientation of the planar diffusion.

The high-contrast colors were chosen to emphasize the transition between linear and planar regions. However, the colors are just used as enhancement of information that is already contained in the texture. Using a black-white color transition as in Fig. 13 is sufficient as well, provided that high image resolution is possible to reveal the fine grass-like structures in the data sets.

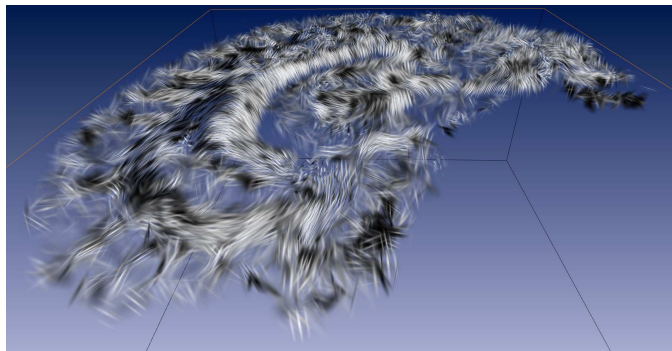


Figure 13: The tensor field looks like grass on a meadow, indicating the preferred direction in the tensor field. If two directions are equivalently preferred, the stalks “smear” into planar leaves.

The tensor splats method extends easily to three-dimensional data sets, although it might require some fine-tuning of the visualization parameters to hide more of the isotropic regions than needed for two-dimensional slices. The full three-dimensional view of the brain data is shown in fig.14, whereas the visual impression is of course increased by high resolution images and direct user interaction with the three-dimensional geometry on a computer screen or VR projection device. The directional information as provided by the tensor splats technique

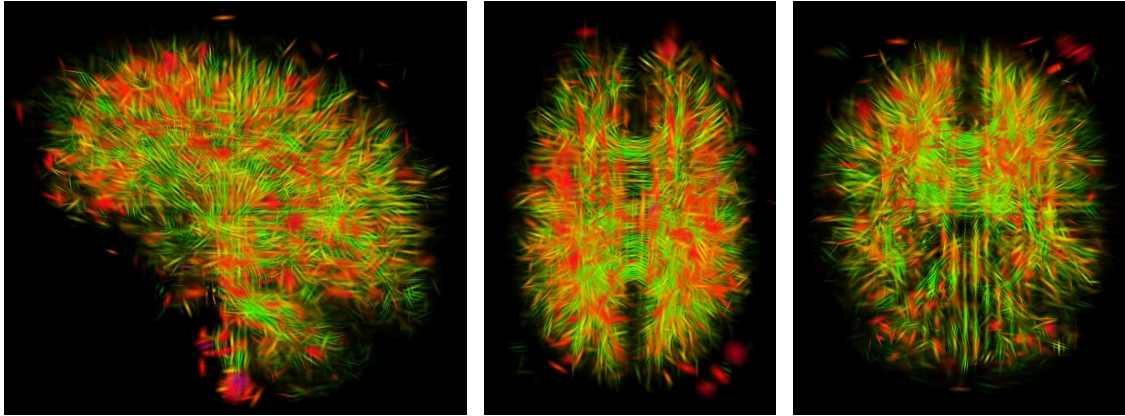


Figure 14: Tensor Splats are capable to visualize an entire 3D volume of the Brain. The third part of the accompanied movie demonstrates a rotation of the data volume.

also easily coexists with standard volume rendering. So beside color coding some scalar or vector field on the tensor splats themselves, a smooth volume rendering may be used in addition to display other scalar quantities. Useful examples are the trace of the tensor field, or the c_1 shape factor field, as shown in Fig. 15 to display the coincidence of highly linear regions and the directional information provided by the tensor splats.

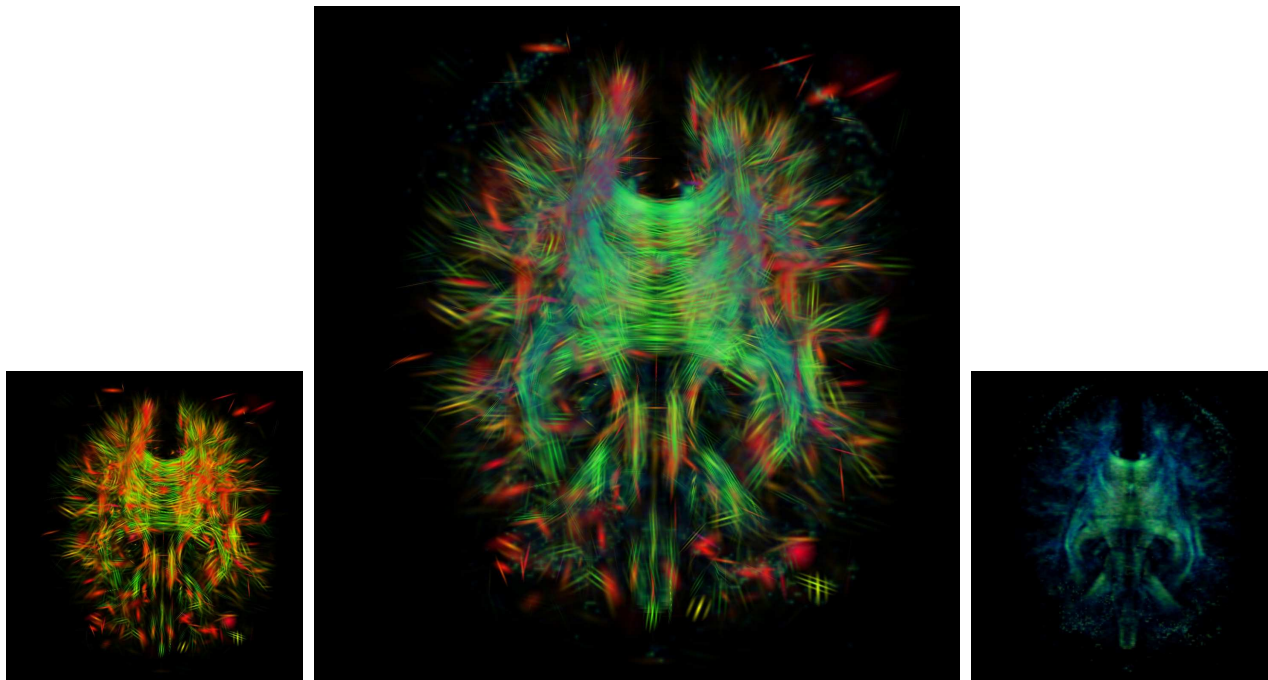


Figure 15: While volume rendering of the anisotropy shape factor c_1 (right) gives a notion *where* some highly linear regions occur, the tensor splatting (left) also gives a notion in *which direction* such a linear diffusion takes place. Both volume rendering and tensor splats can also be combined well into one visualization (center).

6 Acknowledgements

The visualization routines were implemented as an extension to the Amira [8] visualization environment, making use of HDF5 [21] as powerful data format. The data set of orbiting black holes was computed with Cactus [19] by the numerical relativity group at the Max-Planck-Institute for Gravitational Physics in Golm, Germany, using computational resources at the National Center for Supercomputing

Applications. We especially thank Gordon Kindlmann, University of Utah, and Andrew L. Alexander, currently at University of Wisconsin-Madison, for providing the tensor field data of the human brain.

References

- [1] A.L. Alexander, K. Hasan, G. Kindlmann, D.L. Parker, and J.S. Tsuruda. A geometrical analysis of diffusion tensor measurements of the human brain. *Magnetic Resonance in Medicine*, 44:283–291, 2000.
- [2] G. Allen, T. Goodale, G. Lanfermann, E. Seidel, W. Benger, H.-C. Hege, A. Merzky, J. Massó, and J. Shalf. Solving einstein's equation on supercomputers. *IEEE Computer*, 32(12):52–59, December 1999. http://www.computer.org/computer/articles/einstein_1299_1.htm.
- [3] W. Benger. Simulation of a black hole by raytracing. In R.A. Puntigam, F.W. Hehl, and H. Ruder, editors, *Relativity and Scientific Computing - Computer Algebra, Numerics, Visualization*, pages 2–3, Berlin Heidelberg New York, 1996. Springer Verlag. <http://www.photon.at/~werner/bh/>.
- [4] M. Bondarescu, M. Alcubierre, and E. Seidel. Isometric embeddings of black hole horizons in three-dimensional flat space. *Class.Quant.Grav.*, 19, 2002. <http://arxiv.org/abs/gr-qc/0109093>.
- [5] E. Boring. Visualization of tensor fields. Master's thesis, University of California, Santa Cruz, 1998.
- [6] E. Boring and A. Pang. Interactive deformations from tensor fields. In *Visualization '98*, pages 297–304, June 1998.
- [7] S. Bryson. Virtual spacetime: An environment for the visualization of curved spacetimes via geodesic flows. In *Visualization '92*, pages 291–298. Boston, 1992.
- [8] Indeed Visual Concepts. The amira visualization environment. <http://www.amiravis.com/>, 2003.
- [9] R.A. Crawfis and N. Max. Textured splats for 3d scalar and vector field visualization. In Nielson and Bergeron, editors, *Visualization '93, San Jose*, pages 261–266. IEEE CS Press, 1993.
- [10] T. Delmarcelle and L. Hesselink. Visualizing second order tensor fields with hyperstream lines. *IEEE Computer Graphics and Applications*, 13:25–33, July 1993.
- [11] R.B. Haber. Visualization techniques for engineering mechanics. *Comp. Sys. in Engineering*, 1(1):37–50, 1990.
- [12] I. Hotz. Isometric embedding by surface reconstruction from distances. In *Visualization 2002*, pages 251–257, 2002.
- [13] V. Interrante and C. Grosch. Strategies for effectively visualizing 3d flow with volume lic. In *Visualization '97*, pages 421–424. ACM Press, 1997.
- [14] G. Kindlmann and D. Weinstein. Hue-balls and lit-tensors for direct volume rendering of diffusion tensor fields. In *Visualization '99*, pages 183 – 189, 1999.
- [15] G. Kindlmann, D. Weinstein, and D. Hart. Strategies for direct volume rendering of diffusion tensor fields. *IEEE Transactions on Visualization and Computer Graphics*, 6(2):124–138, 2000.
- [16] R.D. Kriz, E.H. Glaessgen, and J.D. MacRae. Eigenvalue-eigenvector glyphs: Visualizing zeroth, second, fourth and higher order tensors in a continuum. *Workshop on Modeling the Development of Residual Stresses During Thermoset Composite Curing*, September 1995. Report No. 95-19.
- [17] D.H. Laidlaw, E.T. Ahrens, D. Kremers, M. J. Avalos, R. E. Jacobs, and C. Readhead. Visualizing diffusion tensor images of the mouse spinal cord. pages 127–134, June 1998.
- [18] J. Li, H.-Y. Shum, and Q. Peng. An improved spacetime ray tracing system for the visualization of relativistic effects. In *Eurographics 2001 (short presentation)*, 2001.
- [19] Max-Planck-Institute for Gravitational Physics. The cactus computational toolkit. <http://www.cactuscode.org/>, 2003.
- [20] J.G. Moore, S.A. Schorn, and J. Moore. Methods of classical mechanics applied to turbulence stresses in a tip leakage vortex. In *Proceedings of the ASME Gas Turbine Conference, Houston, Texas*, number 95-GT-220, 1995.
- [21] NCSA. Hierarchical data format version 5. <http://hdf5.ncsa.uiuc.edu/hdf5/>, 2003. National Center for Supercomputing Applications.
- [22] H.P. Nollert and H. Herold. Visualization in curved spacetimes - visualization of surfaces via embeddings. In F.E. Hehl, R.A. Puntigam, and H. Ruder, editors, *Relativity and Scientific Computing*, pages 330–351. Springer Verlag, 1996.
- [23] J.D. Romano and R.H. Price. Embedding initial data for black-hole collisions. *Class. Quantum Grav.*, 12:875–894, 1995. <http://arxiv.org/abs/gr-qc/9409047>.
- [24] B.F. Schutz. *Gravity from the Ground Up*. Cambridge University Press, 2003.
- [25] G.S. Settles. *Schlieren and Shadowgraph Techniques: Visualizing Phenomena in Transparent Media*. Springer Verlag, 2001. <http://web.mit.edu/edgerton/people/vandiver/schlieren.html>.
- [26] A. Sigfridsson, T. Ebbens, E. Heiberg, and L. Wigstroem. Tensor field visualization using adaptive filtering of noise fields combined with glyph rendering. In *Visualization 2002*, pages 371–378, 2002.
- [27] D. Stalling. *Fast Texture-Based Algorithms for Vector Field Visualization*. PhD thesis, Free University Berlin, 1998.
- [28] D. Weinstein, G. Kindlmann, and E. Lundberg. Tensorlines: Advection-diffusion based propagation through diffusion tensor fields. In *IEEE Visualization 1999*, pages 249–253. IEEE Computer Society Press, 1999.
- [29] D. Weiskopf. Four-Dimensional Non-Linear Ray Tracing as a Visualization Tool for Gravitational Physics. In T. Ertl, B. Hamann, and A. Varshney, editors, *Visualization '00*, pages 445–448. ACM Press, Oct. 2000.
- [30] C.F. Westin, S.E. Maier, B. Khidir, P. Everett, F.A. Jolesz, and R. Kikinis. Image processing for diffusion tensor magnetic resonance imaging. In editors Taylor C, Colchester A, editor, *MICCAI 99: Second International Conference on Medical Image Computing and Computer-Assisted Intervention*, pages 441–452. Springer Verlag, Heidelberg, Germany, 1999.
- [31] C.F. Westin, S. Peled, H. Gudbjartsson, R. Kikinis, and F.A. Jolesz. Geometrical diffusion measures for mri from tensor basis analysis. In *Proceedings of ISMRM, Fifth Meeting, Vancouver, Canada*, page 1742, April 1997.
- [32] X. Zheng and A. Pang. Volume deformation for tensor visualization. In *Visualization 2002*, pages 379–386, 2002.
- [33] X. Zheng and A. Pang. Interaction of light and tensor fields. In *Vis.Sym '03*, pages 157 – 166, 2003.
- [34] L. Zhukov, K. Museth, D. Breen, R. Whitaker, and A. Barr. Level set segmentation and modeling of dt-mri human brain data. *Journal of Electronic Imaging*, 12(1):125–133, 2003.